K^0_S and Λ production in quark and gluon jets at LEP

M. Acciarri, O. Adriani, M. Aguilar-Benitez, S. Ahlen, J. Alcaraz, G. Alemanni, J. Allaby, A. Aloisio, G. Alverson, M G. Alviggi, et al.

EUROPEAN ORGANIZATION FOR NUCLEAR RESEARCH

CERN-PPE/97-50
7 May 1997

K^0_s and Λ Production in Quark and Gluon Jets at LEP

The L3 Collaboration

Abstract

A measurement of the K^0_s and Λ inclusive production rates and momentum spectra in two- and three-jet events is presented. On the basis of about 3.1 million Z decays collected with the L3 detector at LEP, we observe that the production of these particles is well modelled by string fragmentation.

Submitted to *Phys. Lett. B*

1 Introduction

Hadronic Z decays provide important data to study the process of hadronization, which is too complex to be calculated in detail by perturbative QCD. Presently, it is only described by phenomenological models. Recently, we have shown experimental evidence for differences in hadronization of quarks and gluons: The production of η mesons was found to be harder than expected in jets originating from the fragmentation of gluons [1].

In this paper, we measure the production of K^0_s mesons and Λ ($\bar{\Lambda}$) [1)] baryons in two-jet events and in quark and gluon jets from three-jet events. Comparison of K^0_s, Λ and charged particles may reveal differences in hadronization due to the strange quark as well as to the mesonic and baryonic nature of these particles.

2 Data and Monte Carlo Samples

The analysed data, collected by the L3 detector [2] at LEP ($\sqrt{s} \approx 91$ GeV), correspond to an integrated luminosity of 112 pb^{-1}. The selection of hadronic Z decays is based on the energy measured in the electromagnetic and hadron calorimeters. Events must have more than 12 calorimetric clusters. The total visible energy, E_vis, the transverse and longitudinal energy imbalances, $E_\perp$ and $E_\parallel$, must satisfy the following conditions:

$$0.5 < \frac{E_\mathrm{vis}}{\sqrt{s}} < 2.0 \quad ; \quad \frac{E_\perp}{E_\mathrm{vis}} < 0.5 \quad \text{and} \quad \frac{|E_\parallel|}{E_\mathrm{vis}} < 0.5.$$

About 3.1 million events are accepted. The trigger efficiency for these events is 99.9%.

The JETSET 7.3 program [3] is used to generate Monte Carlo events. The generated events are passed through the full detector simulation [4] which takes into account the effects of energy loss, multiple scattering, interactions and decays inside the detector materials. The efficiency to accept hadronic Z decays is found to be 99.0%.

For comparison with another hadronization model, the HERWIG 5.9 event generator [5] is used. Its main difference with JETSET is that the hadronization of partons is modelled by cluster fragmentation instead of string fragmentation.

3 Measurement of Production Rates

The charged particle reconstruction is based on a Time Expansion Chamber surrounded by a Z Chamber and, since 1994, on a Silicon Microvertex Detector [6, 7]. To be selected, tracks must reach the central part of the detector ($40^\circ < \theta < 140^\circ$) and have a transverse momentum greater than 150 MeV.

3.1 Secondary Vertex Selection

For the reconstruction of secondary vertices, V^0, selected tracks are accepted according to the following criteria:

- The distance of closest approach to the nominal beam position of each track, projected onto the transverse plane, must be greater than 0.5 mm. This value is large enough to

[1)] In the following, Λ will refer to both Λ and $\bar{\Lambda}$.

remove tracks originating from short-lived particle decays and small enough to retain efficiency for tracks resulting from secondary vertices of K^0_s or Λ. The beam position is determined on a fill-by-fill basis.

- The transverse distance of flight, defined by the secondary vertex position with respect to the beam axis, must be greater than 5 mm. This removes background from short-lived particles.

- The angle between the direction of the transverse momentum of the track pairs and the transverse flight direction is required to be smaller than 200 mrad. This eliminates combinations of tracks not pointing to the beam axis.

3.2 K^0_s and Λ Measurement

The K^0_s candidates are reconstructed by calculating the invariant mass of oppositely charged tracks, assuming each track to be a pion. For the Λ reconstruction, the proton mass is assigned to the track with the highest momentum. K^0_s candidates with a scaled momentum x_p smaller than 0.005, where x_p is defined as the reconstructed momentum divided by the beam energy, are rejected. This threshold is increased to 0.01 for Λ baryons to exclude photon conversions. The combinatorial background distributions are obtained by combining tracks with the same charge. These distributions are corrected on an event-by-event basis for the difference between the number of like and unlike sign combinations. Without this correction, the combinatorial backgrounds would be underestimated by about 3% and the results overestimated by 0.4%.

The $\pi^+\pi^-$ and $p\pi^-(\bar{p}\pi^+)$ mass distributions, after subtraction of the combinatorial background, are shown in Figure 1, both for the data and simulation. The hatched histograms in Figure 1 show the expected contributions of K^0_s, Λ and $\gamma \to e^+e^-$. These mass distributions are mainly populated by secondary vertex candidates. Other contributions to the background are found to be less than 0.5%.

As shown in the Monte Carlo distributions of Figure 1a, the $\pi^+\pi^-$ mass distribution includes mainly K^0_s but also has some contribution from Λ. The $p\pi$ mass distribution in Figure 1b shows, besides the Λ signal, a strong K^0_s contribution and a small contribution from $\gamma \to e^+e^-$ conversions.

The number of K^0_s and Λ in the Monte Carlo distributions, inside the mass windows 0.3–0.8 GeV and 1.07–1.17 GeV of Figure 1a and Figure 1b respectively, are rescaled to fit the data. The fractions of expected K^0_s and Λ in these distributions, as well as the magnitude of other background contributions, mainly photon conversions, are kept fixed. The scale factors so obtained are used to calculate the production rates of K^0_s and Λ in the data. The resulting total numbers of particles reconstructed in the above-mentioned mass intervals are $(560.0 \pm 1.5) \times 10^3$ K^0_s and $(88.0 \pm 0.9) \times 10^3$ Λ. Including correction for neutral decays, the total acceptances are 18% and 8% for K^0_s and Λ, respectively.

3.3 K^0_s and Λ Momentum Spectra

The procedure described in section 3.2 has been repeated for different K^0_s and Λ momenta. The resulting differential inclusive production rates are shown in Figure 2a for the K^0_s , and Figure 2b for the Λ. The shape for K^0_s is in reasonable agreement with both Monte Carlo expectations while the Λ production rate at low momentum is underestimated by JETSET and overestimated by HERWIG. The inclusive production rates have also been measured as a

function of the variable $\xi = -\log(x_p)$. These distributions are shown in Figure 2c for K^0_s and Figure 2d for Λ. They have been fitted in the indicated region using the distorted Gaussian function expected in the Modified Leading Log Approximation (MLLA) [8]. The chosen region is the largest with a small χ^2. We find a maximum at $\xi^*_{K^0_s}=2.76\pm0.04$ for K^0_s and $\xi^*_\Lambda=2.78\pm0.05$ for Λ baryons.

The spectra have been integrated in order to obtain the total inclusive production rates. After extrapolation to the full phase space, we obtain the following average multiplicities per event:

$$< K^0_s >_{\rm total} = 1.012 \pm 0.003({\rm stat.}) \pm 0.021({\rm syst.})\ \ K^0_s/{\rm event},$$

$$< \Lambda >_{\rm total} = 0.364 \pm 0.004({\rm stat.}) \pm 0.017({\rm syst.})\ \ \Lambda/{\rm event}.$$

Both multiplicity and ξ^* measurements are in good agreement with our previous measurement [9] and with results of other LEP experiments [10–12]. These production rates can be compared with the Monte Carlo predictions which are respectively 1.024 K^0_s/event and 0.347 Λ/event with JETSET, and 1.041 K^0_s/event and 0.378 Λ/event with HERWIG. The expected values for ξ^* from JETSET (HERWIG) are $\xi^*_{K^0_s}=2.71$ (2.77) and $\xi^*_\Lambda=2.60$ (2.83).

	K^0_s	Λ
Tracking acceptance and efficiency	1.3%	1.5%
Secondary vertex selection and background	1.5%	2.9%
Λ reflection, K^0_s reflection, $\gamma \to e^+e^-$	0.6%	3.3%
Monte Carlo Statistics	0.3%	1.3%
Total	2.1%	4.8%

Table 1: Contributions to the total systematic uncertainty on average multiplicities.

The quoted systematic uncertainty on the presented average multiplicities is the quadratic sum of different contributions as shown in Table 1. The main contribution to the systematic error arises from the selection procedure for tracks and secondary vertices. The measurements have been repeated varying the selection criteria described in section 3.1. Changing the charged particle momentum threshold and extending the polar angle acceptance introduces an error of 1.3% (1.5%) for K^0_s (Λ). Small errors in the extrapolation to the full phase space are also included. Bhabha events have been used to correct Monte Carlo tracking efficiency. Removing one by one the cuts to accept secondary vertex candidates increases the background by more than a factor two, whereas the measured rate does not change by more than 1.4% for K^0_s and 2.7% for Λ. Including an uncertainty of 0.5% (1.1%) found by comparing total rates with the sum of those obtained in two- and three-jet events (see next section) where the event topology is different, we get a total uncertainty of 1.5% (2.9%). Tests with Monte Carlo simulation have shown that the measurements are not sensitive to a wrong number of generated charged particles, K^0_s or Λ. In the case of the K^0_s, the uncertainty in the background originating from the measured Λ production rate is 0.6%. For the Λ, the corresponding uncertainty due to K^0_s is 3.3%. An uncertainty of 10% in the rate of photon conversions has a negligible effect on the results.

4 Production Rates within Jets

4.1 Jet Reconstruction

The LUCLUS jet finder algorithm [3, 13] is used to reconstruct jet energies and directions. Calorimetric clusters of energy and direction $\vec{E}_i$ and $\vec{E}_j$ are joined to a single cluster with energy and direction $\vec{E}_i+\vec{E}_j$ if the distance d_{ij} defined by

$$d_{ij} = 2\frac{E_i E_j \sin(\theta_{ij}/2)}{E_i + E_j}$$

is smaller than a given value $d_{\rm join}$. The angle between the two clusters is denoted by θ_{ij}. This procedure is repeated recursively to join all possible pairs of clusters. The final resulting clusters are called jets. The parameter $d_{\rm join}$ is fixed to 7 GeV. The fraction of two-jet events is found to be 70.6% in the data and 69.8% (70.5%) in the simulation based on JETSET (HERWIG). Events with more than two jets are classified as three-jet events.

In three-jet events, jets are sorted according to their energy ($E_1 > E_2 > E_3$). The reconstructed jet energy distributions are shown in Figure 3. We observe good agreement between data and simulation. Using the JETSET program in Matrix Element mode, the probability that the least energetic jet originates from gluon fragmentation is found to be 72%, while the probability that the most energetic jet originates from one of the primary quarks is larger than 90%. Hence, the two most energetic jets are referred to as quark jets while the remaining jets are called gluon jets.

The flow of the sum of $\rm K^0_s$ and Λ ($\rm V^0$) and of charged particles in three-jet events, is compared with the simulation in Figure 4. The charged particles used in this comparison are selected with the same track selection described in section 3. The number of charged particles includes tracks from decays of neutral particles like $\rm K^0_s$, Λ and π^0 Dalitz decays, but it has been corrected for electrons coming from photon conversions. The comparison is performed in the event plane of the three-jet events. This plane is defined by the axis of the quark jets, in their rest frame, and the direction of the third jet. The distribution of the angle, defined such that jet 1, the most energetic jet, is at 0°, jet 2 at 180° and jet 3 between 180° and 360°, of the particle trajectories projected onto this plane is shown in Figure 4a for the sum of $\rm K^0_s$ and Λ, and in Figure 4b for charged particles. The particle distributions within jets are well reproduced by our simulations. Slight differences are observed in the region between the two quark jets opposite to the third jet, which is sensitive to the "string effect" [14]. In this region, the data for charged particles and for the sum of $\rm K^0_s$ and Λ are consistent with each other. One also notes that the enhancement corresponding to gluon jets is more marked for neutral particles associated to $\rm V^0$ than for charged particles. According to JETSET, this is due to Λ production.

4.2 Measurements within Jets

Production rates in two- and three-jet events are measured using the same procedure as for the total event sample in section 3. The differential production rates for $\rm K^0_s$ and Λ are shown in Figure 5. For both particles, the distributions show harder momentum spectra in two-jet events than in three-jet events. The ratios, $\rm R_{32}$, of the total rates measured in three-jet events over that the total rates in two-jet events are found to be $\rm R_{32}(K^0_s)$=1.30±0.02 and $\rm R_{32}(\Lambda)$=1.40±0.04. A similar increase is also observed for charged particles for which $\rm R_{32}(N_{ch})$ is 1.36±0.01. Higher

particle production is expected from QCD for gluon jets because the colour charge of gluons is larger than that of quarks. This effect is implemented in JETSET as well as in HERWIG. The Monte Carlo expectations from JETSET are $R_{32}(K^0_s)$=1.26, $R_{32}(\Lambda)$=1.42 and $R_{32}(N_{ch})$=1.30. They are in good agreement with our measurements. The charged particle production ratio is reasonably well reproduced by HERWIG with $R_{32}(N_{ch})$=1.30, but its predictions for K^0_s and Λ, $R_{32}(K^0_s)$= 1.12 and $R_{32}(\Lambda)$= 1.19, disagree with the data. The expected higher multiplicity in three-jet events leads to lower average particle momentum and hence to softer spectra and higher value of ξ^*. This is indeed observed (see Table 2) and reasonably well reproduced by both JETSET and HERWIG.

For three-jet events, we compare production rates in gluon jets with those in quark jets. To measure the rates within jets, particles are associated to the closest jet in the laboratory frame. The differential production rates are presented in Figure 6a and Figure 6b. For K^0_s, the shapes of the measured spectra are in good agreement with JETSET for both types of jet. Slightly softer distributions are again observed for Λ, except for the gluon jets, where the rate is in better agreement at low x_p than for quark jets. With HERWIG for both K^0_s and Λ, we observe general agreement in quark jets, but the spectra are softer in the gluon jets.

Measured as a function of ξ, the distributions, shown in Figure 6c and Figure 6d, have a maximum ξ^* (see Table 2) shifted toward higher values in gluon jets relative to quark jets. This is qualitatively reproduced by both JETSET and HERWIG. The value of ξ^* for gluon jets is much greater than for quark jets or than all events although the energy is much lower. This is in contrast to the relationship $\xi^* \propto \sqrt{s}$ experimentally observed for all events [8].

	$\xi^*_{K^0_s}$			ξ^*_{Λ}		
	DATA	JETSET	HERWIG	DATA	JETSET	HERWIG
All events	2.76±0.04	2.71	2.77	2.78±0.05	2.60	2.83
Two-jet events	2.60±0.04	2.50	2.54	2.57±0.13	2.35	2.78
Three-jet events	2.99±0.04	2.99	3.09	2.90±0.05	2.70	2.86
- Quark jets	2.81±0.04	2.69	2.80	2.81±0.07	2.45	2.67
- Gluon jets	3.28±0.03	3.28	3.47	3.01±0.05	2.92	3.06

Table 2: Position of the maxima ξ^* in the different event configurations for K^0_s and Λ. Uncertainties are statistical and systematic.

The spectra are integrated to determine the rates of K^0_s and Λ per jet. Then, the rates are divided by the total inclusive production rates measured in section 3. These relative production rates, i.e, the ratio of the rate per jet to the rate per event in the total sample, are more accurate because many of the systematic uncertainties cancel in the ratio. These relative rates are given in Table 3. Good agreement is found between data and JETSET expectations. However, HERWIG differs markedly from the data.

The corresponding rates for charged particles are given in the last columns of Table 3 with their respective Monte-Carlo expectations. The data agree with the predictions of both JETSET and HERWIG.

In three-jet events, we can compare rates in gluon jets with those measured in quark jets by forming the relevant ratios. For K^0_s, we observe that the rate in gluon jets is about (13±3)% lower than in quark jets. The same reduction, (13±1)%, is measured for charged particles. A reduction of (8±5)% is found for Λ. These reductions are well reproduced by JETSET. HERWIG predicts larger reductions for K^0_s and Λ, namely 29% and 19%, respectively.

	$\frac{<K^0_s>_{perjet}}{<K^0_s>_{total}}$			$\frac{<\Lambda>_{perjet}}{<\Lambda>_{total}}$			$\frac{<N_{ch}>_{perjet}}{<N_{ch}>_{total}}$		
	DATA	JETSET	HERWIG	DATA	JETSET	HERWIG	DATA	JETSET	HERWIG
Two-jet events	0.460±0.004	0.464	0.481	0.451±0.011	0.444	0.470	0.460±0.001	0.460	0.455
Three-jet events	0.399±0.005	0.391	0.360	0.421±0.013	0.423	0.375	0.400±0.001	0.398	0.395
- Quark jets	0.417±0.009	0.413	0.400	0.436±0.014	0.426	0.400	0.417±0.001	0.416	0.412
- Gluon jets	0.361±0.007	0.347	0.281	0.403±0.015	0.417	0.326	0.363±0.001	0.358	0.361
$1-\frac{Rate_{InGluonJet}}{Rate_{InQuarkJet}}$	$(13 \pm 3)\%$	16%	29%	$(8 \pm 5)\%$	2%	19%	$(13.0 \pm 1)\%$	14%	12%

Table 3: Measured relative rates for K^0_s, Λ and charged particles observed in different species of jets and events with their respective Monte Carlo expectations. Uncertainties are statistical and systematic added in quadrature.

4.2 Comparison with the Rates of Charged Particles

The observed reduction of particle production in gluon jets is expected to be mainly due to the reduced phase space available during the fragmentation. However, this reduction is partially compensated by an increase of particle production from gluon fragmentation relative to quark fragmentation due to the higher colour charge of gluons. Hence, in order to investigate a possible difference in the K^0_s and Λ production in gluon jets related to the nature of these particles rather than to the jet energy, a comparison is made with the rate of charged particles.

Table 4 shows the ratios, $R(K^0_s)$ and $R(\Lambda)$, of the rates of K^0_s and Λ to that of charged particles, normalised to the same ratio measured per event:

$$R(K^0_s) = \frac{\frac{<K^0_s>_{perjet}}{<N_{ch}>_{perjet}}}{\frac{<K^0_s>_{total}}{<N_{ch}>_{total}}} \quad \text{and} \quad R(\Lambda) = \frac{\frac{<\Lambda>_{perjet}}{<N_{ch}>_{perjet}}}{\frac{<\Lambda>_{total}}{<N_{ch}>_{total}}}. \qquad (1)$$

The measured ratio $R(K^0_s)$ is similar in gluon jets and in quark jets, whereas $R(\Lambda)$ is greater in the gluon jets. This is reproduced by JETSET but not by HERWIG.

	$R(K^0_s)$			$R(\Lambda)$		
	DATA	JETSET	HERWIG	DATA	JETSET	HERWIG
Two-jet events	1.00±0.01	1.01	1.06	0.98±0.03	0.96	1.03
Three-jet events	1.00±0.01	0.98	0.91	1.05±0.03	1.06	0.95
- Quark jets	1.00±0.02	0.99	0.97	1.05±0.04	1.02	0.97
- Gluon jets	1.00±0.01	0.97	0.78	1.11±0.04	1.16	0.90

Table 4: The relative production rates, $R(K^0_s)$ and $R(\Lambda)$, observed in the different species of jets and events with their Monte Carlo expectations. Uncertainties are statistical and systematic added in quadrature.

In Figure 7, we plot the dependence of R on the scaled jet energy ($2E_{\rm jet}/E_{\rm vis}$) for K^0_s and Λ in three-jet events. The distributions for K^0_s and Λ are different. Whereas $R(K^0_s)$ is almost independent of energy, $R(\Lambda)$ increases significantly at both low and high energies. Data and JETSET are in reasonable agreement for both K^0_s and Λ, but HERWIG fails to describe $R(K^0_s)$

and R(Λ) for the low energetic jets, where the enrichement in gluon jets is the highest. Similar observations have recently also been made by the DELPHI collaboration [15].

These relative rate variations seen for Λ are well reproduced by JETSET. This agreement is obtained by the presence of different processes which contribute to the baryon production. The increase of Λ baryon production in the less energetic jets with respect to charged particles is modelled by JETSET with a larger diquark production relative to quark production at lower energy. This is obtained with a diquark fragmentation function which is softer than the one for quarks. No increase is expected from the HERWIG program in which no specific process such as diquark production is implemented. In the JETSET program, the increase of quark production with energy also favours "popcorn" processes [3]. This qualitatively explains the increase of the relative rates observed in highly energetic jets. In HERWIG, cluster fragmentation makes the particle production mainly dependent on the available phase space. Hence, the production of the lightest particles is favoured in the least energetic jets.

5 Conclusion

We have measured production of K_s^0 and Λ in hadronic Z decays, and their production in two-jet events and within three-jet events have been compared. The overall agreement between data and simulation based on string fragmentation is good, both for quark jet and gluon jet samples. For K_s^0 mesons, this illustrates that the production of strange quarks relative to other light quarks does not differ significantly between quark and gluon fragmentation. For Λ baryons, differences are observed. They can be explained by the specific energy dependence of the production processes for baryons as implemented in the JETSET model. There is no need to invoke differences in quark and gluon fragmentation beyond those implied by string fragmentation.

Acknowledgements

We wish to express our gratitude to the CERN accelerator divisions for the excellent performance of the LEP machine. We acknowledge with appreciation the effort of all engineers, technicians and support staff who have participated in the construction and maintenance of this experiment. Those of us who are not from member states thank CERN for its hospitality and help.

The L3 Collaboration:

M.Acciarri,[28] O.Adriani,[17] M.Aguilar-Benitez,[27] S.Ahlen,[11] J.Alcaraz,[27] G.Alemanni,[23] J.Allaby,[18] A.Aloisio,[30] G.Alverson,[12] M.G.Alviggi,[30] G.Ambrosi,[20] H.Anderhub,[50] V.P.Andreev,[39] T.Angelescu,[13] F.Anselmo,[9] A.Arefiev,[29] T.Azemoon,[3] T.Aziz,[10] P.Bagnaia,[38] L.Baksay,[45] R.C.Ball,[3] S.Banerjee,[10] Sw.Banerjee,[10] K.Banicz,[47] A.Barczyk,[50,48] R.Barillère,[18] L.Barone,[38] P.Bartalini,[35] A.Baschirotto,[28] M.Basile,[9] R.Battiston,[35] A.Bay,[23] F.Becattini,[17] U.Becker,[16] F.Behner,[50] J.Berdugo,[27] P.Berges,[16] B.Bertucci,[35] B.L.Betev,[50] S.Bhattacharya,[10] M.Biasini,[18] A.Biland,[50] G.M.Bilei[35] J.J.Blaising,[4] S.C.Blyth,[36] G.J.Bobbink,[2] R.Bock,[1] A.Böhm,[1] L.Boldizsar,[14] B.Borgia,[38] A.Boucham,[4] D.Bourilkov,[50] M.Bourquin,[20] D.Boutigny,[4] S.Braccini,[20] J.G.Branson,[41] V.Brigljevic,[50] I.C.Brock,[36] A.Buffini,[17] A.Buijs,[46] J.D.Burger,[16] W.J.Burger,[20] J.Busenitz,[45] X.D.Cai,[16] M.Campanelli,[50] M.Capell,[16] G.Cara Romeo,[9] G.Carlino,[30] A.M.Cartacci,[17] J.Casaus,[27] G.Castellini,[17] F.Cavallari,[38] N.Cavallo,[30] C.Cecchi,[20] M.Cerrada,[27] F.Cesaroni,[24] M.Chamizo,[27] Y.H.Chang,[52] U.K.Chaturvedi,[19] S.V.Chekanov,[32] M.Chemarin,[26] A.Chen,[52] G.Chen,[7] G.M.Chen,[7] H.F.Chen,[21] H.S.Chen,[7] M.Chen,[16] G.Chiefari,[30] C.Y.Chien,[5] L.Cifarelli,[40] F.Cindolo,[9] C.Civinini,[17] I.Clare,[16] R.Clare,[16] H.O.Cohn,[33] G.Coignet,[4] A.P.Colijn,[2] N.Colino,[27] V.Commichau,[1] S.Costantini,[8] F.Cotorobai,[13] B.de la Cruz,[27] A.Csilling,[14] T.S.Dai,[16] R.D'Alessandro,[17] R.de Asmundis,[30] A.Degré,[4] K.Deiters,[48] P.Denes,[37] F.DeNotaristefani,[38] D.DiBitonto,[45] M.Diemoz,[38] D.van Dierendonck,[2] F.Di Lodovico,[50] C.Dionisi,[38] M.Dittmar,[50] A.Dominguez,[41] A.Doria,[30] I.Dorne,[4] M.T.Dova,[19,♯] E.Drago,[30] D.Duchesneau,[4] P.Duinker,[2] I.Duran,[42] S.Dutta,[10] S.Easo,[35] Yu.Efremenko,[33] H.El Mamouni,[26] A.Engler,[36] F.J.Eppling,[16] F.C.Erné,[2] J.P.Ernenwein,[26] P.Extermann,[20] M.Fabre,[48] R.Faccini,[38] S.Falciano,[38] A.Favara,[17] J.Fay,[26] O.Fedin,[39] M.Felcini,[50] B.Fenyi,[45] T.Ferguson,[36] F.Ferroni,[38] H.Fesefeldt,[1] E.Fiandrini,[35] J.H.Field,[20] F.Filthaut,[36] P.H.Fisher,[16] I.Fisk,[41] G.Forconi,[16] L.Fredj,[20] K.Freudenreich,[50] C.Furetta,[28] Yu.Galaktionov,[29,16] S.N.Ganguli,[10] P.Garcia-Abia,[49] S.S.Gau,[12] S.Gentile,[38] J.Gerald,[5] N.Gheordanescu,[13] S.Giagu,[38] S.Goldfarb,[23] J.Goldstein,[11] Z.F.Gong,[21] A.Gougas,[5] G.Gratta,[34] M.W.Gruenewald,[8] V.K.Gupta,[37] A.Gurtu,[10] L.J.Gutay,[47] B.Hartmann,[1] A.Hasan,[31] D.Hatzifotiadou,[9] T.Hebbeker,[8] A.Hervé,[18] W.C.van Hoek,[32] H.Hofer,[50] S.J.Hong,[44] H.Hoorani,[36] S.R.Hou,[52] G.Hu,[5] V.Innocente,[18] H.Janssen,[4] K.Jenkes,[1] B.N.Jin,[7] L.W.Jones,[3] P.de Jong,[18] I.Josa-Mutuberria,[27] A.Kasser,[23] R.A.Khan,[19] D.Kamrad,[49] Yu.Kamyshkov,[33] J.S.Kapustinsky,[25] Y.Karyotakis,[4] M.Kaur,[19,◇] M.N.Kienzle-Focacci,[20] D.Kim,[38] D.H.Kim,[44] J.K.Kim,[44] S.C.Kim,[44] Y.G.Kim,[44] W.W.Kinnison,[25] A.Kirkby,[34] D.Kirkby,[34] J.Kirkby,[18] D.Kiss,[14] W.Kittel,[32] A.Klimentov,[16,29] A.C.König,[32] A.Kopp,[49] I.Korolko,[29] V.Koutsenko,[16,29] R.W.Kraemer,[36] W.Krenz,[1] A.Kunin,[16,29] P.Ladron de Guevara,[27] G.Landi,[17] C.Lapoint,[16] K.Lassila-Perini,[50] P.Laurikainen,[22] M.Lebeau,[18] A.Lebedev,[16] P.Lebrun,[26] P.Lecomte,[50] P.Lecoq,[18] P.Le Coultre,[50] C.Leggett,[3] J.M.Le Goff,[18] R.Leiste,[49] E.Leonardi,[38] P.Levtchenko,[39] C.Li,[21] C.H.Lin,[52] W.T.Lin,[52] F.L.Linde,[2,18] L.Lista,[30] Z.A.Liu,[7] W.Lohmann,[49] E.Longo,[38] W.Lu,[34] Y.S.Lu,[7] K.Lübelsmeyer,[1] C.Luci,[38] D.Luckey,[16] L.Luminari,[38] W.Lustermann,[48] W.G.Ma,[21] M.Maity,[10] G.Majumder,[10] L.Malgeri,[38] A.Malinin,[29] C.Maña,[27] D.Mangeol,[32] S.Mangla,[10] P.Marchesini,[50] A.Marin,[11] J.P.Martin,[26] F.Marzano,[38] G.G.G.Massaro,[2] D.McNally,[18] S.Mele,[30] L.Merola,[30] M.Meschini,[17] W.J.Metzger,[32] M.von der Mey,[1] Y.Mi,[23] A.Mihul,[13] A.J.W.van Mil,[32] G.Mirabelli,[38] J.Mnich,[18] P.Molnar,[8] B.Monteleoni,[17] R.Moore,[3] S.Morganti,[38] T.Moulik,[10] R.Mount,[34] S.Müller,[1] F.Muheim,[20] A.J.M.Muijs,[2] S.Nahn,[16] M.Napolitano,[30] F.Nessi-Tedaldi,[50] H.Newman,[34] T.Niessen,[1] A.Nippe,[1] A.Nisati,[38] H.Nowak,[49] Y.D.Oh,[44] H.Opitz,[1] G.Organtini,[38] R.Ostonen,[22] C.Palomares,[27] D.Pandoulas,[1] S.Paoletti,[38] P.Paolucci,[30] H.K.Park,[36] I.H.Park,[44] G.Pascale,[38] G.Passaleva,[17] S.Patricelli,[30] T.Paul,[12] M.Pauluzzi,[35] C.Paus,[1] F.Pauss,[50] D.Peach,[18] Y.J.Pei,[1] S.Pensotti,[28] D.Perret-Gallix,[4] B.Petersen,[32] S.Petrak,[8] A.Pevsner,[5] D.Piccolo,[30] M.Pieri,[17] J.C.Pinto,[36] P.A.Piroué,[37] E.Pistolesi,[28] V.Plyaskin,[29] M.Pohl,[50] V.Pojidaev,[29,17] H.Postema,[16] N.Produit,[20] D.Prokofiev,[39] G.Rahal-Callot,[50] N.Raja,[10] P.G.Rancoita,[28] M.Rattaggi,[28] G.Raven,[41] P.Razis,[31] K.Read,[33] D.Ren,[50] M.Rescigno,[38] S.Reucroft,[12] T.van Rhee,[46] S.Riemann,[49] K.Riles,[3] O.Rind,[3] A.Robohm,[50] J.Rodin,[16] B.P.Roe,[3] L.Romero,[27] S.Rosier-Lees,[4] Ph.Rosselet,[23] W.van Rossum,[46] S.Roth,[1] J.A.Rubio,[18] D.Ruschmeier,[8] H.Rykaczewski,[50] J.Salicio,[18] E.Sanchez,[27] M.P.Sanders,[32] M.E.Sarakinos,[22] S.Sarkar,[10] M.Sassowsky,[1] G.Sauvage,[4] C.Schäfer,[1] V.Schegelsky,[39] S.Schmidt-Kaerst,[1] D.Schmitz,[1] P.Schmitz,[1] M.Schneegans,[4] N.Scholz,[50] H.Schopper,[51] D.J.Schotanus,[32] J.Schwenke,[1] G.Schwering,[1] C.Sciacca,[30] D.Sciarrino,[20] L.Servoli,[35] S.Shevchenko,[34] N.Shivarov,[43] V.Shoutko,[29] J.Shukla,[25] E.Shumilov,[29] A.Shvorob,[34] T.Siedenburg,[1] D.Son,[44] A.Sopczak,[49] V.Soulimov,[30] B.Smith,[16] P.Spillantini,[17] M.Steuer,[16] D.P.Stickland,[37] H.Stone,[37] B.Stoyanov,[43] A.Straessner,[1] K.Strauch,[15] K.Sudhakar,[10] G.Sultanov,[19] L.Z.Sun,[21] G.F.Susinno,[20] H.Suter,[50] J.D.Swain,[19] X.W.Tang,[7] L.Tauscher,[6] L.Taylor,[12] Samuel C.C.Ting,[16] S.M.Ting,[16] M.Tonutti,[1] S.C.Tonwar,[10] J.Tóth,[14] C.Tully,[37] H.Tuchscherer,[45] K.L.Tung,[7] Y.Uchida,[16] J.Ulbricht,[50] U.Uwer,[18] E.Valente,[38] R.T.Van de Walle,[32] G.Vesztergombi,[14] I.Vetlitsky,[29] G.Viertel,[50] M.Vivargent,[4] R.Völkert,[49] H.Vogel,[36] H.Vogt,[49] I.Vorobiev,[29] A.A.Vorobyov,[39] A.Vorvolakos,[31] M.Wadhwa,[6] W.Wallraff,[1] J.C.Wang,[16] X.L.Wang,[21] Z.M.Wang,[21] A.Weber,[1] F.Wittgenstein,[18] S.X.Wu,[19] S.Wynhoff,[1] J.Xu,[11] Z.Z.Xu,[21] B.Z.Yang,[21] C.G.Yang,[7] X.Y.Yao,[7] J.B.Ye,[21] S.C.Yeh,[52] J.M.You,[36] An.Zalite,[39] Yu.Zalite,[39] P.Zemp,[50] Y.Zeng,[1] Z.Zhang,[7] Z.P.Zhang,[21] B.Zhou,[11] Y.Zhou,[3] G.Y.Zhu,[7] R.Y.Zhu,[34] A.Zichichi,[9,18,19] F.Ziegler.[49]

1 I. Physikalisches Institut, RWTH, D-52056 Aachen, FRG§
III. Physikalisches Institut, RWTH, D-52056 Aachen, FRG§
2 National Institute for High Energy Physics, NIKHEF, and University of Amsterdam, NL-1009 DB Amsterdam, The Netherlands
3 University of Michigan, Ann Arbor, MI 48109, USA
4 Laboratoire d'Annecy-le-Vieux de Physique des Particules, LAPP,IN2P3-CNRS, BP 110, F-74941 Annecy-le-Vieux CEDEX, France
5 Johns Hopkins University, Baltimore, MD 21218, USA
6 Institute of Physics, University of Basel, CH-4056 Basel, Switzerland
7 Institute of High Energy Physics, IHEP, 100039 Beijing, China△
8 Humboldt University, D-10099 Berlin, FRG§
9 University of Bologna and INFN-Sezione di Bologna, I-40126 Bologna, Italy
10 Tata Institute of Fundamental Research, Bombay 400 005, India
11 Boston University, Boston, MA 02215, USA
12 Northeastern University, Boston, MA 02115, USA
13 Institute of Atomic Physics and University of Bucharest, R-76900 Bucharest, Romania
14 Central Research Institute for Physics of the Hungarian Academy of Sciences, H-1525 Budapest 114, Hungary‡
15 Harvard University, Cambridge, MA 02139, USA
16 Massachusetts Institute of Technology, Cambridge, MA 02139, USA
17 INFN Sezione di Firenze and University of Florence, I-50125 Florence, Italy
18 European Laboratory for Particle Physics, CERN, CH-1211 Geneva 23, Switzerland
19 World Laboratory, FBLJA Project, CH-1211 Geneva 23, Switzerland
20 University of Geneva, CH-1211 Geneva 4, Switzerland
21 Chinese University of Science and Technology, USTC, Hefei, Anhui 230 029, China△
22 SEFT, Research Institute for High Energy Physics, P.O. Box 9, SF-00014 Helsinki, Finland
23 University of Lausanne, CH-1015 Lausanne, Switzerland
24 INFN-Sezione di Lecce and Universitá Degli Studi di Lecce, I-73100 Lecce, Italy
25 Los Alamos National Laboratory, Los Alamos, NM 87544, USA
26 Institut de Physique Nucléaire de Lyon, IN2P3-CNRS,Université Claude Bernard, F-69622 Villeurbanne, France
27 Centro de Investigaciones Energeticas, Medioambientales y Tecnologicas, CIEMAT, E-28040 Madrid, Spain♭
28 INFN-Sezione di Milano, I-20133 Milan, Italy
29 Institute of Theoretical and Experimental Physics, ITEP, Moscow, Russia
30 INFN-Sezione di Napoli and University of Naples, I-80125 Naples, Italy
31 Department of Natural Sciences, University of Cyprus, Nicosia, Cyprus
32 University of Nijmegen and NIKHEF, NL-6525 ED Nijmegen, The Netherlands
33 Oak Ridge National Laboratory, Oak Ridge, TN 37831, USA
34 California Institute of Technology, Pasadena, CA 91125, USA
35 INFN-Sezione di Perugia and Universitá Degli Studi di Perugia, I-06100 Perugia, Italy
36 Carnegie Mellon University, Pittsburgh, PA 15213, USA
37 Princeton University, Princeton, NJ 08544, USA
38 INFN-Sezione di Roma and University of Rome, "La Sapienza", I-00185 Rome, Italy
39 Nuclear Physics Institute, St. Petersburg, Russia
40 University and INFN, Salerno, I-84100 Salerno, Italy
41 University of California, San Diego, CA 92093, USA
42 Dept. de Fisica de Particulas Elementales, Univ. de Santiago, E-15706 Santiago de Compostela, Spain
43 Bulgarian Academy of Sciences, Central Lab. of Mechatronics and Instrumentation, BU-1113 Sofia, Bulgaria
44 Center for High Energy Physics, Korea Adv. Inst. of Sciences and Technology, 305-701 Taejon, Republic of Korea
45 University of Alabama, Tuscaloosa, AL 35486, USA
46 Utrecht University and NIKHEF, NL-3584 CB Utrecht, The Netherlands
47 Purdue University, West Lafayette, IN 47907, USA
48 Paul Scherrer Institut, PSI, CH-5232 Villigen, Switzerland
49 DESY-Institut für Hochenergiephysik, D-15738 Zeuthen, FRG
50 Eidgenössische Technische Hochschule, ETH Zürich, CH-8093 Zürich, Switzerland
51 University of Hamburg, D-22761 Hamburg, FRG
52 High Energy Physics Group, Taiwan, China

§ Supported by the German Bundesministerium für Bildung, Wissenschaft, Forschung und Technologie
‡ Supported by the Hungarian OTKA fund under contract numbers T14459 and T24011.
♭ Supported also by the Comisión Interministerial de Ciencia y Tecnología
♯ Also supported by CONICET and Universidad Nacional de La Plata, CC 67, 1900 La Plata, Argentina
♢ Also supported by Panjab University, Chandigarh-160014, India
△ Supported by the National Natural Science Foundation of China.

References

[1] L3 Collaboration, M. Acciarri *et al.*, Phys. Lett. **B 371** (1996) 126.

[2] L3 Collaboration, B. Adeva *et al.*, Nucl. Instr. Meth. **A 289** (1990) 35;
L3 Collaboration, B. Adriani *et al.*, Phys. Rep. **236** (1993) 1.

[3] JETSET Monte Carlo program.
T. Sjöstrand, Comp. Phys. Comm. **82** (1994) 74;
T. Sjöstrand, Lund and CERN Preprints LU TP 95-20/CERN-TH.7112/93 (revised, 1995).
The parameters of JETSET have been tuned in order to reproduce event shape variables as seen by the L3 detector. The production of particles (tensor mesons) with orbital angular momentum is enabled. For the tuning see:
L3 Collaboration, B. Adeva *et al.*, Z. Phys. **C 55** (1992) 39.

[4] The L3 detector simulation is based on GEANT
see R. Brun et al, GEANT 3, CERN DD/EE/84-1 (revised, Sept 1987).
The GHEISHA program is used to simulated hadronic interactions
see H. Fesefeld, RWTH Aachen report PITHA 85/02(1985).

[5] HERWIG Monte Carlo program:
G. Marchesini and B. Webber, Nucl. Phys. **B 310** (1988) 461;
I.G. Knowles, Nucl. Phys. **B 310** (1988) 571;
G. Marchesini *et al.*, Comp. Phys. Comm. **67** (1992) 465.
The parameters of HERWIG have been tuned in order to reproduce event shape variables as seen by the L3 detector. The used parameters are: CLMAX=3.052, QCDLAM=0.183, VPCUT=.4 and CLPOW=2.221.

[6] F. Beissel *et al.*, Nucl. Instr. Meth. **A 332** (1993) 33.

[7] L3 Collaboration, M. Acciarri *et al.*, Nucl. Instr. Meth. **A 351** (1994) 300.

[8] Y.L. Dokshitzer, V.A. Khoze and V.A. Troyan, Z. Phys. **C 55** (1992) 107.

[9] L3 Collaboration, M. Acciarri *et al.*, Phys. Lett. **B 328** (1994) 223.

[10] ALEPH Collaboration, D. Buskulic *et al.*, Z. Phys. **C 64** (1994) 361.

[11] DELPHI Collaboration, P. Abreu *et al.*, Z. Phys. **C 65** (1995) 587.

[12] OPAL Collaboration, A. Ackers *et al.*, Z. Phys **C 67** (1995) 45;
OPAL Collaboration, A. Ackers *et al.*, Z. Phys **C 73** (1997) 569.

[13] T. Sjöstrand, Comp. Phys. Comm. **28** (1983) 229.

[14] Y.I. Azimov, Y.L. Dokshitzer, V.A. Khoze, S.I. Troyan, Phys. Lett. **B 165** (1985) 147.

[15] DELPHI Collaboration, P. Abreu *et al.*, CERN-PPE/96-193, submitted to Phys. Lett. B.

Figure Captions

Figure 1 a) Background subtracted $\pi^+\pi^-$ mass distributions for simulation and data.
b) Background subtracted $\mathrm{p}\pi^- + \bar{\mathrm{p}}\pi^+$ mass distributions for simulation and data.

Figure 2 a) The differential inclusive production rate for K^0_s in the total event sample.
b) The corresponding spectrum for Λ.
c) and d) The distribution of the variable ξ for K^0_s and for Λ respectively.
The total hadronic cross section is denoted by σ_h. Error bars include statistical and systematic uncertainties.

Figure 3 The reconstructed jet energy distributions for the three species of jets in three-jet events.

Figure 4 a) Angular flow distribution in three-jet events for neutral particles decaying in a secondary vertex, V^0. The angle goes from the most energetic jet to the second one (at 180°) then, from the second one to the third and finally back to the first one. The region sensitive to the "string effect" is around 135° and the gluon jet region is found around 200°. The continuous lines stands for the JETSET expectation. The dashed line corresponds to the expected K^0_s contribution.
b) Angular flow distribution for charged particles. The continuous (dashed) line stands for the JETSET (HERWIG) prediction.

Figure 5 a) The differential inclusive production rates for K^0_s in two-jet and three-jet events.
b) The corresponding spectra for Λ.
c) and d) The distribution of the variable ξ for K^0_s and for Λ respectively.
The total hadronic cross section is denoted by σ_h. Error bars include statistical and systematic uncertainties.

Figure 6 a) The differential inclusive production rates for K^0_s in three-jet events for quark and gluon jets separately.
b) The corresponding spectra for Λ.
The result labelled as quark jets is the sum of the rates measured in the two most energetic jets. The difference between the two quark jets were not significant.
c) and d) The distribution of the variable ξ for K^0_s and for Λ respectively.
The total hadronic cross section is denoted by σ_h. Error bars include statistical and systematic uncertainties.

Figure 7 The values of $\mathrm{R}(\mathrm{K}^0_\mathrm{s})$ and $\mathrm{R}(\Lambda)$ as function of the scaled jet energy $(2E_\mathrm{jet}/E_\mathrm{vis})$ in three-jet events. The error bars include statistical and systematic uncertainties.

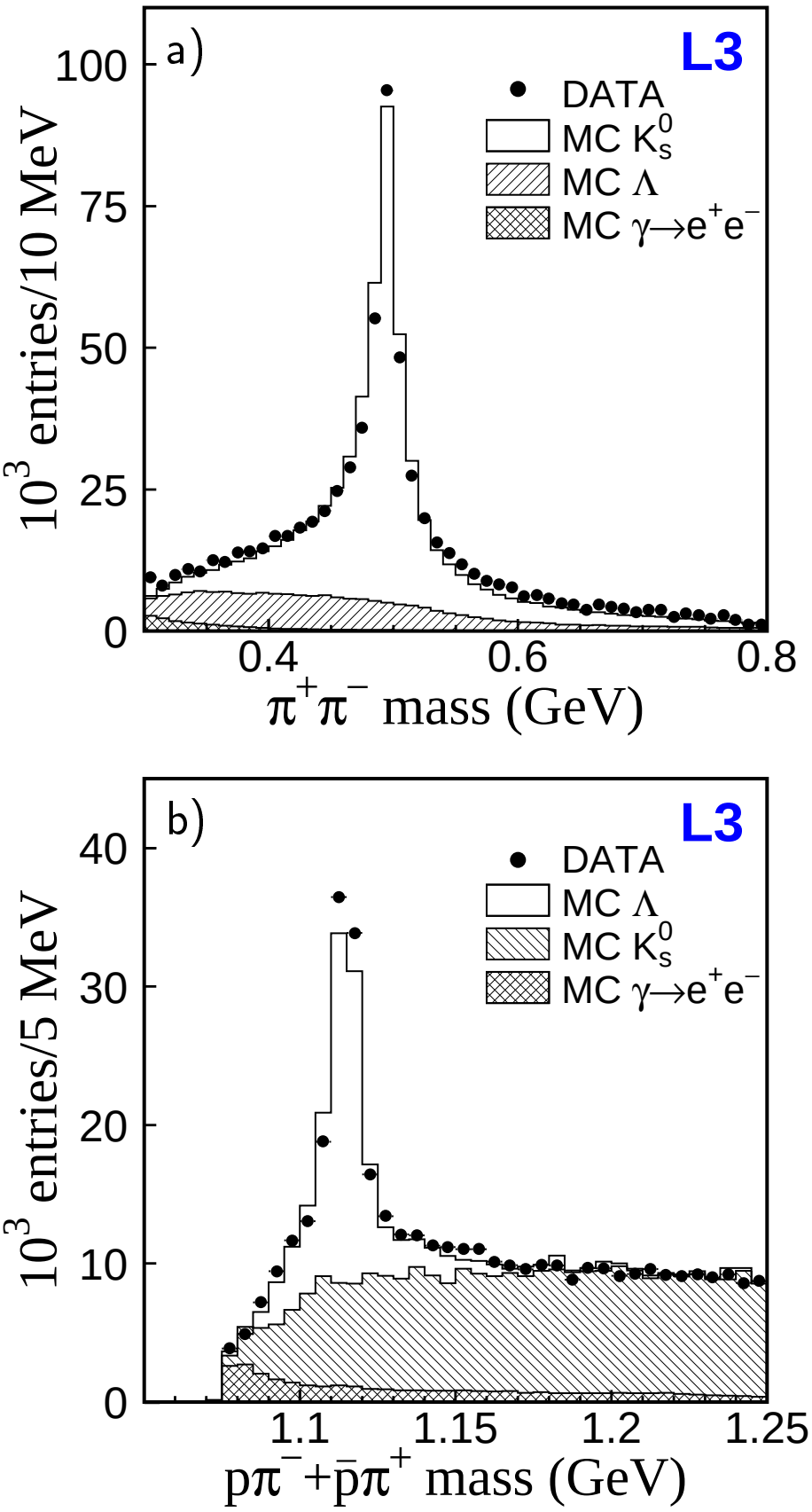

Figure 1: a) Background subtracted $\pi^+\pi^-$ mass distributions for simulation and data. b) Background subtracted $p\pi^- + \bar{p}\pi^+$ mass distributions for simulation and data.

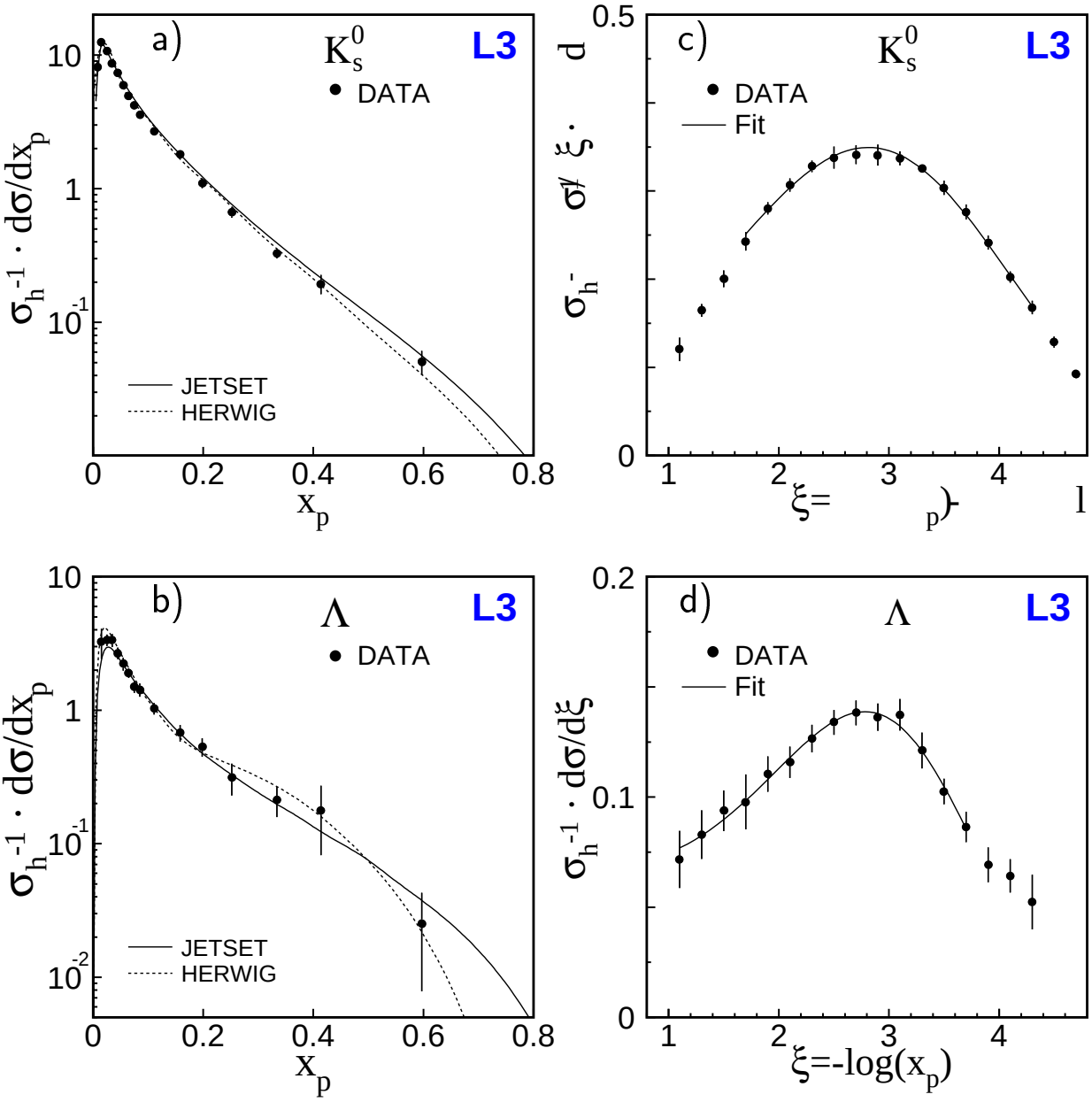

Figure 2: a) The differential inclusive production rate for K_s^0 in the total event sample. b) The corresponding spectrum for Λ. c) and d) The distribution of the variable ξ for K_s^0 and for Λ respectively. The total hadronic cross section is denoted by σ_h. Error bars include statistical and systematic uncertainties.

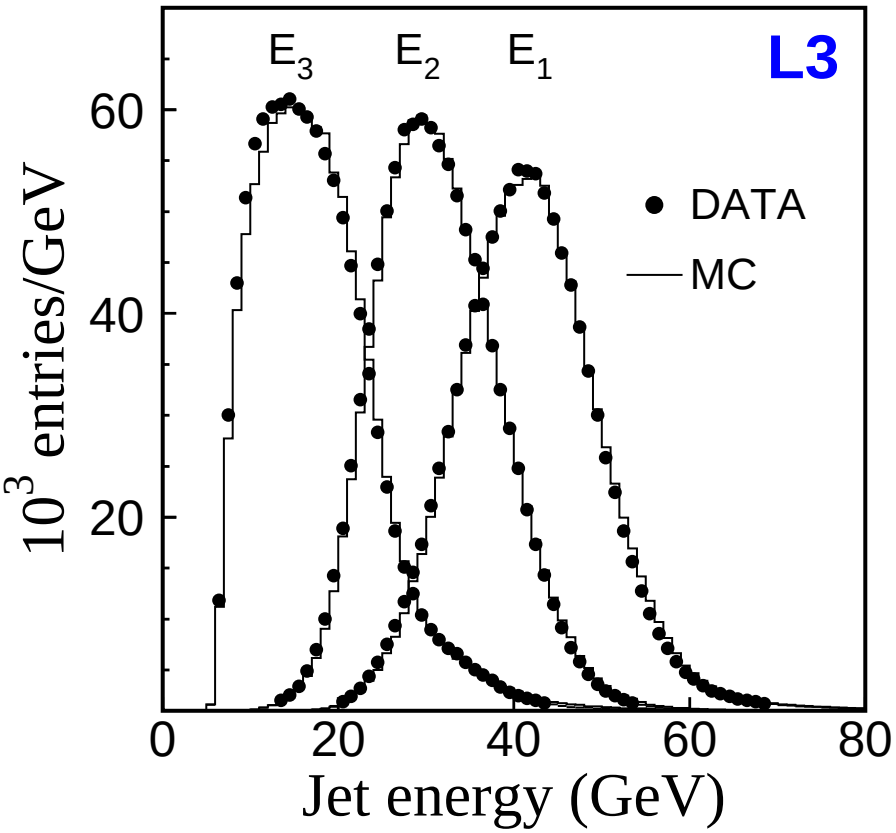

Figure 3: The reconstructed jet energy distributions for the three species of jets in three-jet events.

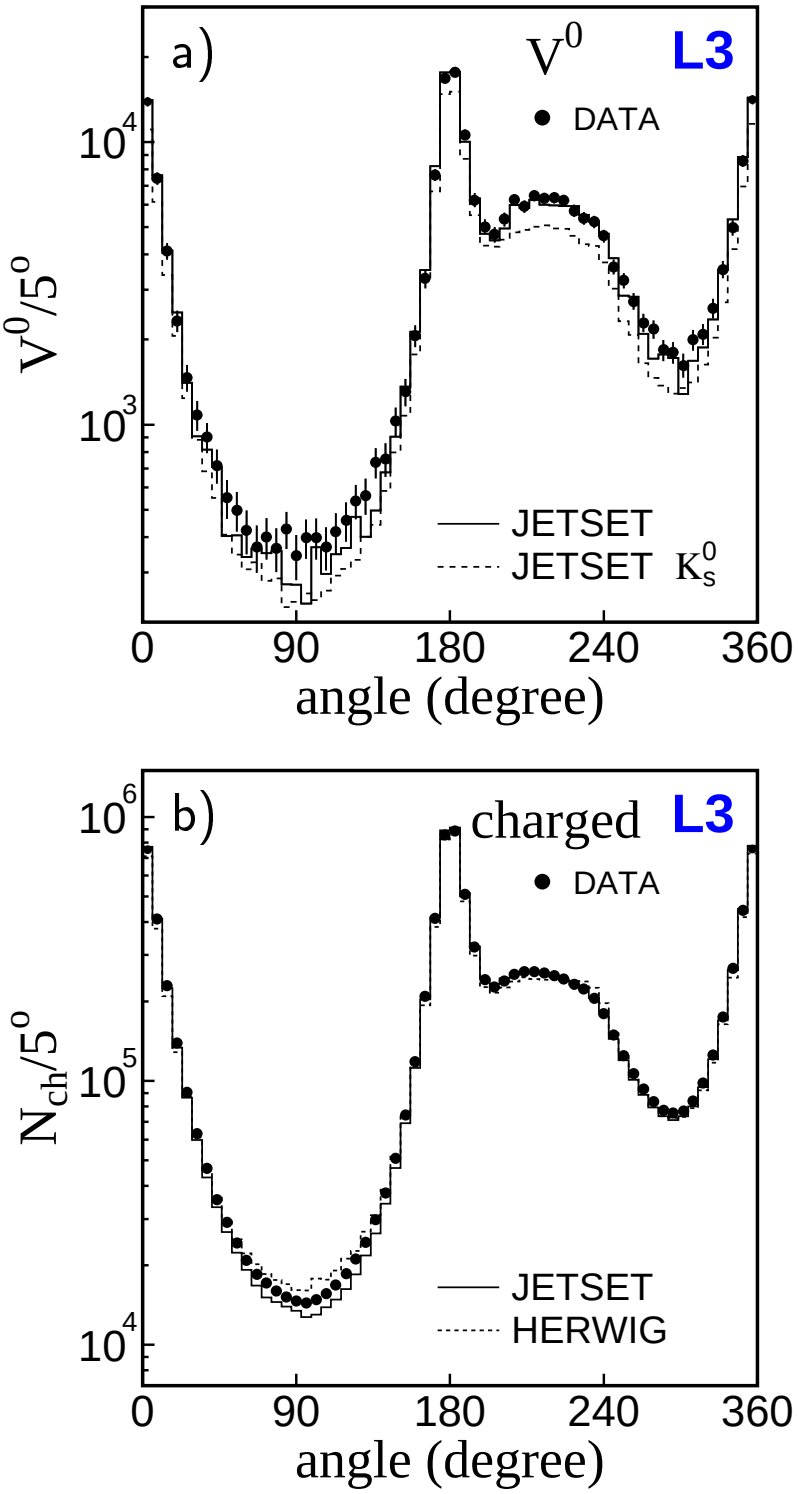

Figure 4: a) Angular flow distribution in three-jet events for neutral particles decaying in a secondary vertex, V^0. The angle goes from the most energetic jet to the second one (at 180°) then, from the second one to the third and finally back to the first one. The region sensitive to the "string effect" is around 135° and the gluon jet region is found around 200°. The continuous lines stands for the JETSET expectation. The dashed line corresponds to the expected K_s^0 contribution. b) Angular flow distribution for charged particles. The continuous (dashed) line stands for the JETSET (HERWIG) prediction.

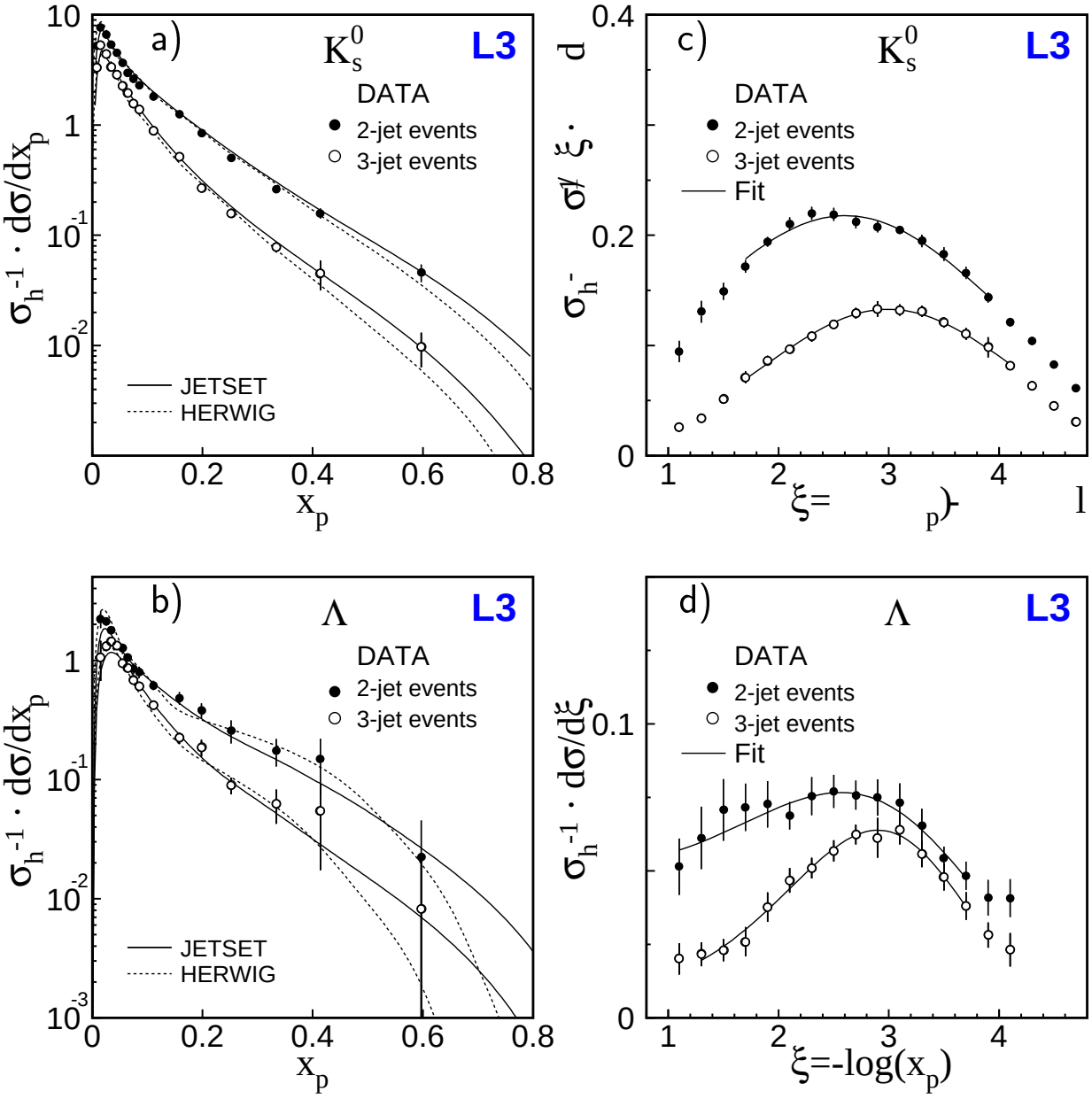

Figure 5: a) The differential inclusive production rates for K^0_s in two-jet and three-jet events. b) The corresponding spectra for Λ. c) and d) The distribution of the variable ξ for K^0_s and for Λ respectively. The total hadronic cross section is denoted by σ_h. Error bars include statistical and systematic uncertainties.

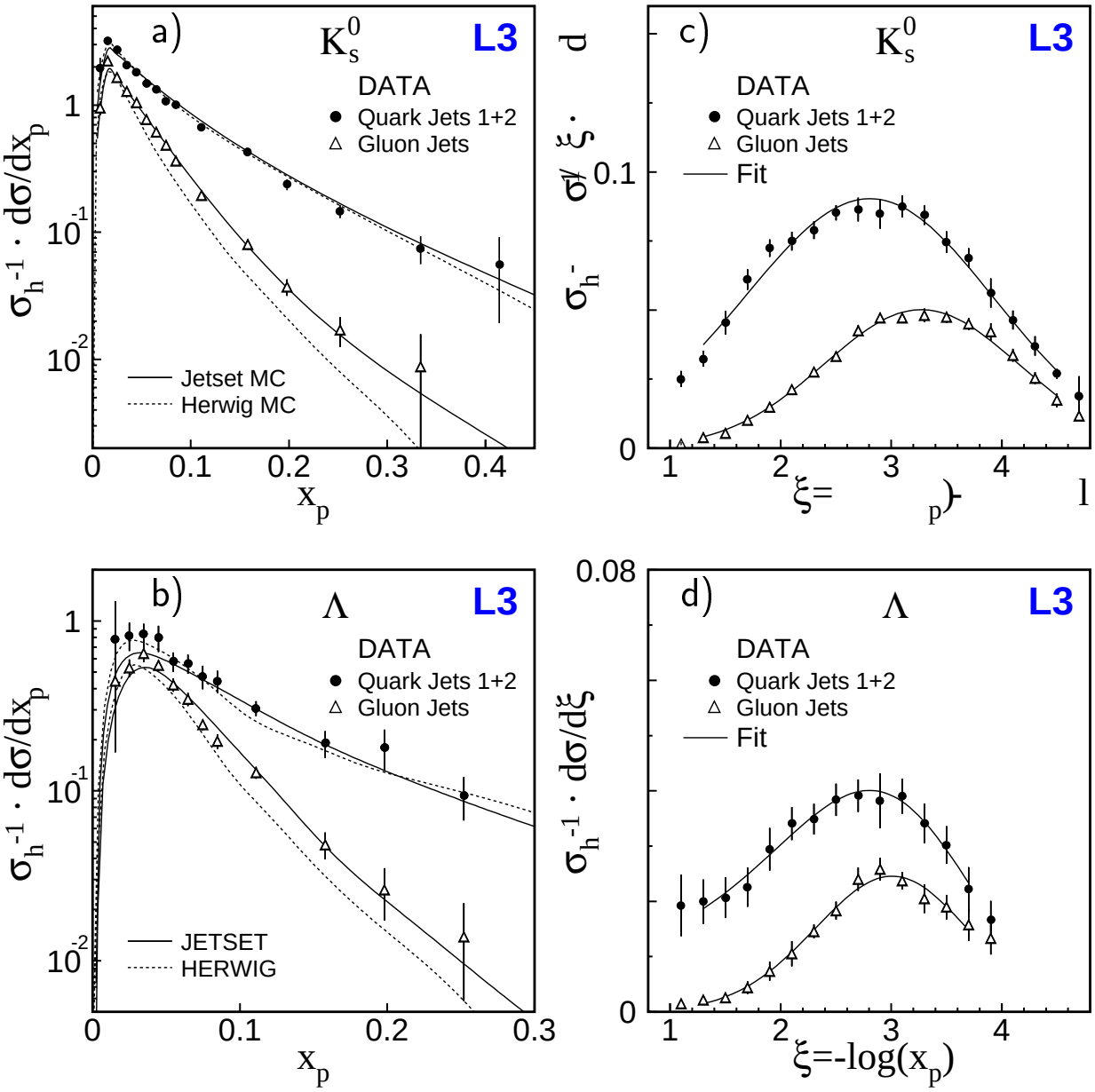

Figure 6: a) The differential inclusive production rates for K^0_s in three-jet events for quark and gluon jets separately. b) The corresponding spectra for Λ. The result labelled as quark jets is the sum of the rates measured in the two most energetic jets. The difference between the two quark jets were not significant. c) and d) The distribution of the variable ξ for K^0_s and for Λ respectively. The total hadronic cross section is denoted by σ_h. Error bars include statistical and systematic uncertainties.

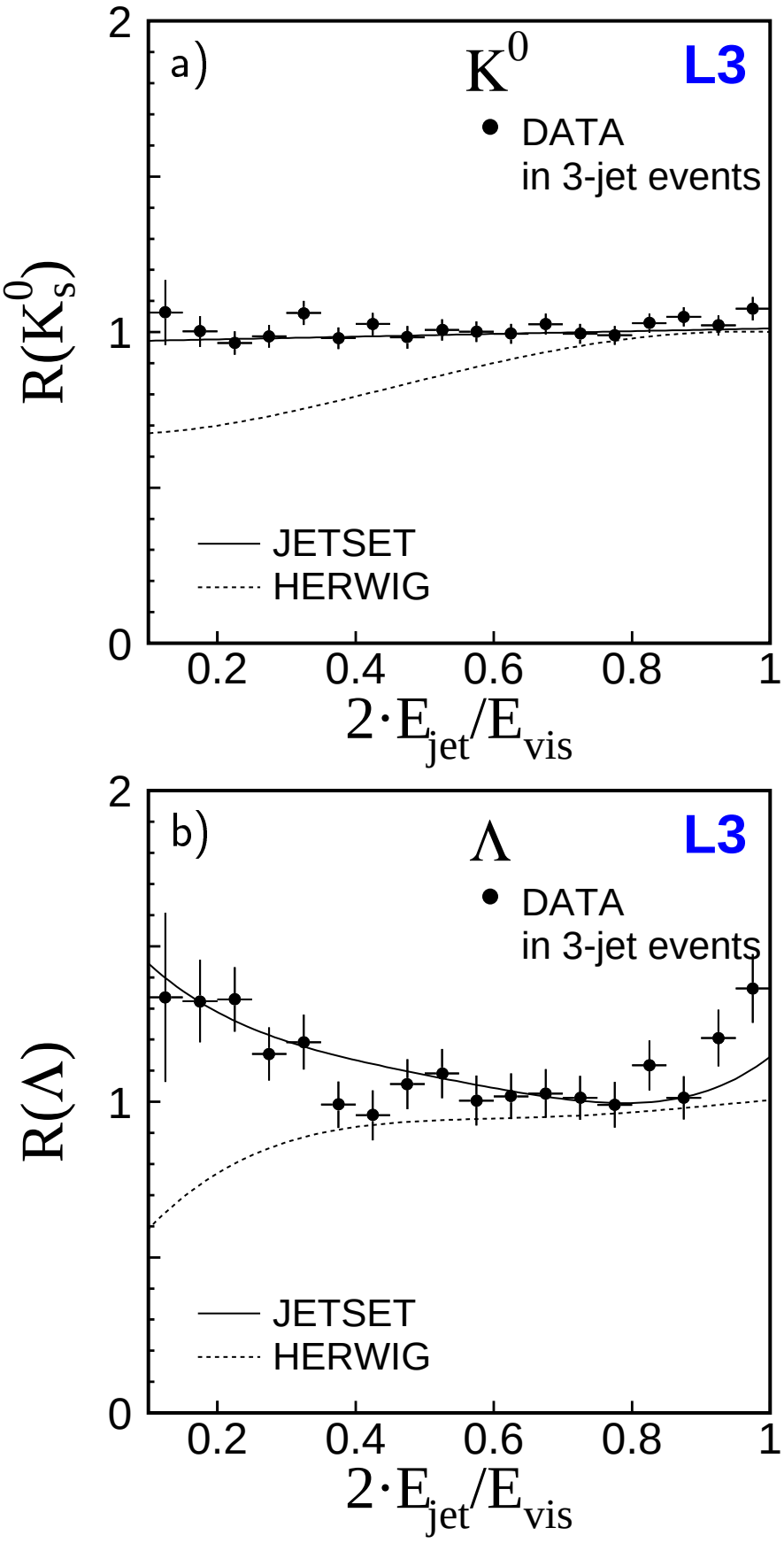

Figure 7: The values of $R(K^0_s)$ and $R(\Lambda)$ as function of the scaled jet energy ($2E_{\rm jet}/E_{\rm vis}$) in three-jet events. The error bars include statistical and systematic uncertainties.